Earth and Planetary Science Letters 527 (2019) 115792

Contents lists available at ScienceDirect

Earth and Planetary Science Letters

www.elsevier.com/locate/epsl

New insights into environmental controls on the occurrence and abundance of Group I alkenones and their paleoclimate applications: Evidence from volcanic lakes of northeastern China

Yuan Yao [a,b], Jiaju Zhao [a], William M. Longo [b], Gaoyuan Li [c], Xian Wang [b], Richard S. Vachula [b], Karen J. Wang [b], Yongsong Huang [a,b,*]

[a] State Key Laboratory of Loess and Quaternary Geology, Institute of Earth Environment, Chinese Academy of Sciences, Xi'an 710061, China
[b] Department of Earth, Environmental and Planetary Sciences, Brown University, Providence, RI 02912, USA
[c] State Key Laboratory of Biogeology and Environmental Geology, China University of Geosciences, Beijing 100083, China

ARTICLE INFO

Article history:
Received 23 March 2019
Received in revised form 9 August 2019
Accepted 25 August 2019
Available online 16 September 2019
Editor: L. Robinson

Keywords:
alkenones
Group I Isochrysidales
DNA
winter temperature proxy
volcanic lakes

ABSTRACT

The distinctive long-chain alkenones (LCAs) produced by Group I Isochrysidales from freshwater and oligohaline lakes have great potential for quantitative paleotemperature reconstructions. The widespread application of sedimentary Group I LCAs, however, is hampered by an incomplete understanding of the environmental controls on the occurrence of Group I LCAs in freshwater lakes. The correspondence between Group I LCA concentrations and pH (6.2–8.5) in northern Alaskan freshwater lakes (Longo et al., 2016) suggests that Group I Isochrysidales may preferentially thrive in freshwater lakes with high pH. Here, we systematically study LCA distributions, haptophyte-specific 18S rDNA sequences, and concentrations of major ions and trace elements in 18 freshwater volcanic lakes in northeastern China with an extended pH range from 7.17 to 9.99. We find that 11 of the 18 lakes examined contain Group I LCAs and the corresponding DNA sequences of their producers. Our DNA results indicate that the dominant alkenone producer in all 11 lakes is closely related to the Group I Greenland OTU 5 genotype, with the exception of two anthropogenically impacted lakes where small numbers of Group II sequences are found. Statistical analyses indicate that the highest concentrations of Group I LCAs are found in oligotrophic freshwater lakes with pH ranging from ~7.3 to 8.8. We find that elevated concentrations of certain trace elements may lead to the disappearance of Group I LCAs despite lake water falling within the optimal pH range. Together with previously published Group I LCA data from the temperature calibration in Northern Hemisphere freshwater lakes (Longo et al., 2018), we find, for the first time, that Group I R3b (R3b = $C_{37:3b}/(C_{38:3b}Et + C_{37:3b})$) values are most sensitive to winter temperature changes when mean winter temperature is higher than ~−20 °C. Our results suggest that the freshwater volcanic lakes in northeastern China are highly valuable targets for paleotemperature reconstructions using Group I LCAs.

1. Introduction

Long-chain alkenones (LCAs) are a class of C_{35}–C_{42} unsaturated methyl (Me) and ethyl (Et) ketones exclusively produced by certain Isochrysidales within haptophyte lineages. In open marine systems, LCAs are ubiquitous (e.g. de Leeuw et al., 1980) and two phylogenetically closely related haptophytes, *Emiliania huxleyi* and *Gephyrocapsa oceanica*, are the dominant producers of C_{37}–C_{39} LCAs (Volkman et al., 1980; Marlowe et al., 1984). A wide range of alkenone studies using culture experiments (e.g. Prahl and Wakeham, 1987; Conte et al., 1998; Zheng et al., 2019), suspended particulate matter (SPM) of marine water (e.g. Conte et al., 1992; Freeman and Wakeham, 1992), and surface sediments (e.g. Conte et al., 2006; Filippova et al., 2016) have demonstrated strong correlations between the C_{37} alkenone unsaturation ratios (U^{K}_{37} and/or $U^{K'}_{37}$) and temperature. The U^{K}_{37} and/or $U^{K'}_{37}$ proxies have been widely used to reconstruct past sea surface temperatures (SST) (e.g. Brassell et al., 1986; Prahl and Wakeham, 1987; Eglinton et al., 1992).

LCAs have also been found to extensively occur in various types of lakes around the world, including freshwater lakes (e.g. Zink et al., 2001; D'Andrea et al., 2016; Longo et al., 2016, 2018), oligoha-

* Corresponding author at: Department of Earth, Environmental and Planetary Sciences, Brown University, Providence, RI 02912, USA.
E-mail address: yongsong_huang@brown.edu (Y. Huang).

https://doi.org/10.1016/j.epsl.2019.115792
0012-821X/

line lakes (e.g. D'Andrea and Huang, 2005; D'Andrea et al., 2006), and saline lakes (e.g. Chu et al., 2005; Liu et al., 2011; Toney et al., 2010; Zhao et al., 2014). Alkenone-producing haptophytes have been divided into the three genetically distinct Isochrysidales groups based on the haptophyte phylogenetic analysis (Theroux et al., 2010): Group I including "Greenland" subclade (D'Andrea et al., 2006; Theroux et al., 2010) and "EV" subclade (Simon et al., 2013; Richter et al., 2019), Group II, and Group III Isochrysidales. These Groups occupy habitats of different salinity, with Group I occurring in freshwater/oligohaline lakes, Group II in saline lakes and coastal seas, and Group III in open ocean environments (Theroux et al., 2010; Longo et al., 2016). Compared with Group III Isochrysidales, Group I and Group II Isochrysidales display higher phylogenetic diversity (Theroux et al., 2010; Richter et al., 2019). To date, there have been no studies successfully isolating and culturing the Group I Isochrysidales, whereas the common Group II species, *Isochrysis galbana*, *Ruttnera* (*Chrysotila*) *lamellosa*, and recently *Tisochrysis Lutea*, have been studied extensively by culture experiments for LCA distributions and temperature calibrations (e.g. Nakamura et al., 2014; Zheng et al., 2016, 2019). The $U^{K''}_{37}$ index has been proposed as the preferred temperature proxy for Group II Isochrysidales due to strengthened temperature correlation after excluding di-unsaturated alkenone in culture experiments (Zheng et al., 2016, 2019). However, Group II LCA distributions and temperature sensitivities are variable among different species or strains (Nakamura et al., 2014; Zheng et al., 2016, 2019), creating significant challenges for quantitative reconstructions of continental paleotemperature using alkenone unsaturation ratios. Nevertheless, recent study by Zhao et al. (2018) demonstrates that shifts in certain Group II Isochrysidales species and the resulting $\%C_{37:4}$ alkenone variations in a hypersaline lake (Gahai) can be used for reconstructing cold season precipitation changes in the northern Qinghai-Tibetan Plateau.

Despite the phylogenetic diversity in Group I Isochrysidales (Richter et al., 2019), the general similarity of Group I LCA distributions suggests that freshwater lakes may be immune to species-mixing effects on unsaturation ratios and are highly valuable targets for quantitative paleotemperature reconstructions (Longo et al., 2016, 2018; Richter et al., 2019). Group I Isochrysidales have been found in freshwater lakes throughout the mid- and high latitudes of the northern hemisphere (Longo et al., 2018). Their presence has been confirmed by DNA evidence in southwestern Greenland (D'Andrea et al., 2006), northeastern Canada (Theroux et al., 2010), France (Simon et al., 2013), Norway (D'Andrea et al., 2016), Japan (Plancq et al., 2018), and northern Alaska (Richter et al., 2019). The LCA profiles of Group I Isochrysidales are characterized by the presence of tri-unsaturated isomers with $\Delta^{14,21,28}$ (instead of the common $\Delta^{7,14,21}$ double bond positions; Longo et al., 2013, 2016) that are absent in Group II and Group III Isochrysidales (Zheng et al., 2019). Their unsaturation ratios correlate strongly with in situ temperatures of water column SPM and sediment trap samples (D'Andrea et al., 2011, 2016; Longo et al., 2016). The Group I U^{K}_{37} values in surface sediments from Northern Hemispheric freshwater lakes are thought to record temperature during the winter-spring transitional season based on its strong correlation with alkenone production and unsaturation ratios (Longo et al., 2018). Importantly, the general consistency of Group I U^{K}_{37}-temperature calibrations from lake water column SPM samples and surface sediments of Northern Hemispheric freshwater lakes reinforces the notion that freshwater lakes may be immune to species-mixing effect (Longo et al., 2016, 2018).

However, not all freshwater lakes host the Group I Isochrysidales, which raises a critical question: what freshwater conditions are suitable for the growth of Group I Isochrysidales? In northern Alaskan freshwater lakes, the concentrations of Group I LCAs are positively related with pH (6.2–8.5), alkalinity and conductivity (Longo et al., 2016), which gives rise to our initial hypothesis that Group I Isochrysidales may preferentially thrive in freshwater lakes with high pH. However, some freshwater lakes with elevated pH do not contain LCAs, indicating that additional environmental factors also play key roles in determining the occurrence of Group I LCAs (Longo et al., 2018). The key environmental controls on presence and absence of Group I LCAs thus are not fully understood.

The presence of a large number of freshwater volcanic lakes with extended high pH range (7.17–9.99) in the volcanic fields of northeastern China provides a potential opportunity to further explore environmental controls on the occurrence, concentrations, and distributions of Group I LCAs. Here we identify Group I Isochrysidales in 11 of 18 freshwater volcanic lakes in northern China by systematically analyzing the DNA sequences of alkenone-producing haptophytes and LCA distributions in surface sediments. Combined with analyses of detailed water chemistry parameters (e.g. pH, common ions, and trace elements), we aim to further constrain environmental factors controlling the presence and concentrations of Group I LCAs, and to identify new potential proxies for paleoclimate applications.

2. Materials and methods

2.1. Study sites and samples

In northeastern China, Cenozoic intraplate volcanism was common and the resulting igneous rocks consist mainly of alkali basalts. There are three main volcanic fields in northeastern China, including Wudalianchi, Longgang (Dragon Mountain Range), and Arxan-Chaihe, which host three corresponding volcanic lake groups (Fig. 1). The Wudalianchi volcanic field, located in north Dedu County of the Heilongjiang province, covers an area of ~720 km^2. It formed in five phases of sequential eruptions during the Quaternary with the latest eruptions occurring in 1719–1721 AD (Laoheishan-Huoshaoshan eruption) and 1776 AD (Laoheishan eruption). Several lava flows dammed the Shilong River, a tributary of the Nemor River, and formed the five dammed lakes of Wudalianchi.

The Longgang volcanic field is located in the northwest of the Sino-Korean border and covers a relatively large area (1700 km^2) with more than 160 Quaternary craters and calderas. There are eight maar lakes (Donglongwan, Nanlongwan, Longquanlongwan, Sanjiaolongwan, Dalongwan, Erlongwan, Xiaolongwan, and Sihailongwan Lake), collectively known as Long Wan Lakes.

The Arxan-Chaihe volcanic field covers an area of ~1000 km^2 in the central segment of the Greater Khingan Mountains. Most volcanic activity in this area occurred during the Pliocene and from the mid- and late-Pleistocene to the Holocene, forming two types of volcanic lakes (crater lakes and dammed lakes).

The climate of the Wudalianchi and Longgang volcanic fields are strongly influenced by the East Asian Summer Monsoon (EASM), whereas the Arxan-Chaihe volcanic field is located on the northern boundary of the modern EASM. The modern climate of the region is characterized by strong seasonality with warm, humid summers and cold, dry winters. The mean annual air temperatures (MAAT; 1979–2013) of the Wudalianchi, Longgang, and Arxan-Chaihe volcanic fields are ~0.4, 2.9, and −2.6 °C, respectively (http://chelsa-climate.org/, Version1.2; Karger et al., 2017). The relatively low temperature for the Arxan-Chaihe volcanic field is mainly due to the comparatively high elevation (~1100 m) relative to Wudalianchi (~300 m) and Long Wan (~700 m). The mean annual precipitation of the three volcanic fields from AD 1970–2003 was ~530, 770, and 440 mm, respectively (http://chelsa-climate.org/, Version1.2; Karger et al., 2017).

We collected surface sediment and water samples from 18 volcanic lakes of three volcanic lake groups (Wudalianchi, Long Wan,

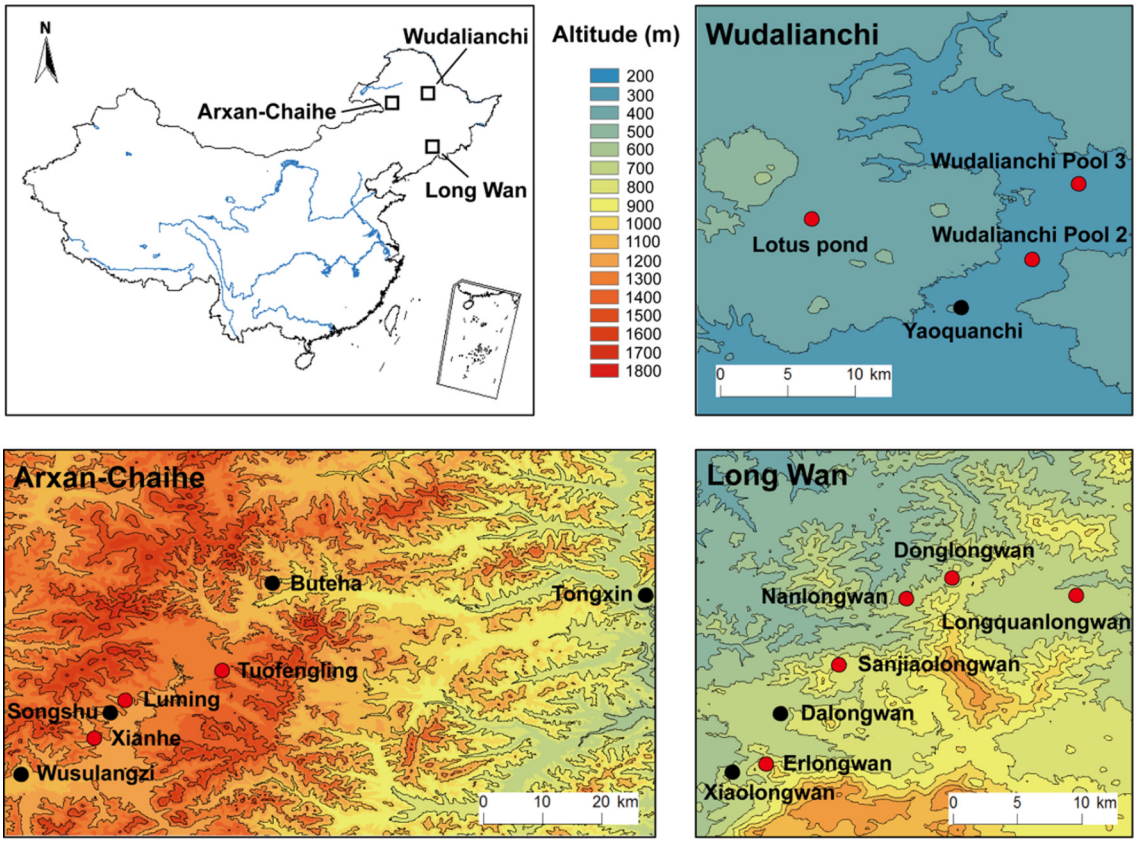

Fig. 1. Geographical map showing the three volcanic lake groups in northeastern China and sampling sites in this study (modified from Yao et al., 2019). The LCA-containing lakes are marked with red circles and the lakes that do not contain LCAs are marked with black circles. (For interpretation of the colors in the figure(s), the reader is referred to the web version of this article.)

and Arxan-Chaihe) in northeastern China in July, 2016 (Fig. 1; Table S1). The surface sediments were sampled into NASCO Whirl-Pak collection bags. The lake water samples for water chemistry analysis were filtered through Whatman GF/F filters (0.7 μm). All collected samples were kept in a cooler with gel ice packs in the field. Then the surface sediment samples for DNA analysis were frozen at −80 °C in the laboratory, the surface sediment sample for LCA analysis were frozen at −20 °C in the laboratory, and the lake water samples were kept in sterile bottles at 4 °C in the laboratory until analysis. Water temperature, pH, and salinity were measured simultaneously with a HACH Hydrolab water analyzer in the field. Three additional surface sediments were collected from volcanic lakes in Southern China (Huguangyan) and Azores (Santiago and Congro).

2.2. Methods

2.2.1. LCAs analysis

All samples for LCA analysis were freeze-dried and extracted by sonication (3×) with dichloromethane (DCM)/methanol (MeOH) (9:1, v/v). The extracts were purified by column chromatography with silica gel using *n*-hexane and dichloromethane (DCM), respectively. The DCM fractions were further purified by column chromatography with silver thiolate silica (Wang et al., 2019). An increasing polarity sequence of solvents (hexane:DCM (2 ml, 2:1, v:v), DCM (1 ml), acetone (2 ml)) was used to separate compounds. All LCAs were retained in the acetone fractions (Zheng et al., 2017; Wang et al., 2019). LCAs were then analyzed by an Agilent 7890N GC system equipped with a flame ionization detector (FID) and a Restek Rtx-200 GC column (105 m × 250 μm × 0.25 μm) at Brown University, USA, as described by Zheng et al. (2017). Prior to LCA analysis, a known amount of 18-pentatricontanone was added to each sample as an internal standard for the quantification of LCAs. The following GC-FID oven program was used: initial temperature of 50 °C (hold 2 min), ramp 20 °C/min to 255 °C, ramp 3 °C/min to 320 °C (hold 25 min).

The RIK_{37} and R3b indices are calculated according to Longo et al. (2016, 2018).

$$RIK_{37} = \frac{[C_{37:3a}]}{[C_{37:3a} + C_{37:3b}]} \quad (1)$$

$$R3b = \frac{[C_{37:3b}]}{[C_{38:3b}Et + C_{37:3b}]} \quad (2)$$

where the "*a*" and "*b*" subscripts refer to the $\Delta^{7,14,21}$ and $\Delta^{14,21,28}$ tri-unsaturated LCAs, respectively.

2.2.2. 18S rDNA analysis

DNA was extracted from ~0.5 g sediment subsamples using the FastDNA SPIN Kit (MP Biomedicals, OH, USA) according to the manufacturer's instructions. The main processes include cell lysis, removal of proteins, and purification of DNA. DNA concentrations were quantified by measuring optical absorbance at 260 nm using a NanoDrop ND-1000 spectrophotometer (Thermo Scientific, Wilmington, USA). Genomic DNA was amplified using haptophyte-specific oligonucleotide primers (Prym-429F: 5′-GCG CGT AAA TTG CCC GAA-3′; Prym-887R: 5′-GGA ATA CGA GTG CCC CTG AC-3′) targeting 18S rDNA coding regions (Coolen et al., 2004). PCR reactions (25 μl volume) contained 16.2 μl double distilled water, 2.5 μl 10 × buffer (TaKaRa Bio, Otsu, Japan), 2 μl dNTP (2.5 mM, TaKaRa Bio, Otsu, Japan), 2 μl a pair of primers (10 μM), 1 μl bovine serum albumin (BSA, 20 mg/ml, TaKaRa Bio, Otsu, Japan), 0.3 μl Ex Taq (5 U/μl, TaKaRa Bio, Otsu, Japan), and 1 μl template sample. All reactions were performed using the following conditions:

4 min initial denaturing at 96 °C, followed by 35 cycles including denaturing (30 s at 94 °C), primer annealing (40 s at 55 °C), and primer extension (40 s at 72 °C), with a final extension of 10 min at 72 °C (Coolen et al., 2004). The PCR amplified 18S rDNA of haptophytes (463 bp) was separated by agarose gel electrophoresis and was then purified using the Nucleic Acid Purification Kit (Axygen, NY, USA) according to the manufacturer's instructions. The purified DNA was cloned with pGEM-T Easy Vector (Promega, WI, USA) and DH5α competent cells according to the manufacturer's instructions. Finally, the cells transformed with vectors containing recombinant DNA (white colonies) using the blue-white screen were sequenced. A blank control was included in all of the above steps, which serves as a control for cross-contamination during the experiments. The DNA experiments were performed at State Key Laboratory of Biogeology and Environmental Geology, China University of Geosciences (Beijing), China.

All obtained DNA sequences were analyzed as queries in Basic Local Alignment Search Tool (BLAST) searches against the National Center for Biotechnology Information (NCBI) database (http://blast.ncbi.nlm.nih.gov/Blast.cgi) with default parameters, and were then removed vector sequences. The operational taxonomic units (OTUs) of all trimmed sequences were determined using the DOTUR software program with a 98% cut-off criterion (Schloss and Handelsman, 2005). Representative sequences for each OTU were chosen and aligned with reference haptophyte sequences from the GeoBank database for phylogenetic tree construction. The neighbor-joining tree was constructed using the molecular evolutionary genetics analysis (MEGA) software with 1000 bootstrap replications. Representative sequences for each OTU in this study have been deposited in GenBank (Accession numbers MN194618-MN194622).

2.2.3. Water chemistry analysis

The total phosphorus (TP) and total nitrogen (TN) of lake water samples were analyzed with inductively coupled plasma-atomic emission spectrometer (ICP-AES) and organic carbon analyzer TOC-V CPH, respectively. Common cations and anions (Cl^-, NO_2^-, NO_3^-, PO_4^{3-}, SO_4^{2-}, Na^+, NH_4^+, K^+, Mg^{2+}, and Ca^{2+}) were analyzed with an ICS-110 ion chromatograph, and trace elements (Fe, Mn, Zn, Cu, Mo, and Co) were analyzed with a Nexion 300D inductively coupled plasma mass spectrometer (ICP-MS) at Institute of Earth Environment, Chinese Academy of Sciences, China.

2.2.4. Statistical analyses

Logistic regressions between OTUs and water chemistry data were performed to analyze the environmental controls on the presence of OTUs using MATLAB. Logistic probability density functions were fitted to alkenone data to determine the pH range for likelihood of the presence and absence of Group I alkenones using MATLAB. Principal components analysis (PCA) was performed to analyze the environmental controls on concentrations of LCAs using the Canoco software version 4.5.

2.2.5. Meteorological data

Monthly temperature and solar radiation data for all sites were extracted from the WorldClim-Global Climate Database (http://www.worldclim.org/version2; Fick and Hijmans, 2017) with 30 seconds (~1 km^2) spatial resolution using the Senckenberg data extraction tool (dataportalsenckenberg.de/dataExtractTool). The mean temperature of the spring isothermal season (MTSI) is calculated as average temperature of the four months centered on the spring isotherm (Longo et al., 2018). MTSI generally represents the temperature during ice melt or ice-off season, which is when Group I Isochrysidales have been found to bloom (D'Andrea et al., 2011; Longo et al., 2016, 2018).

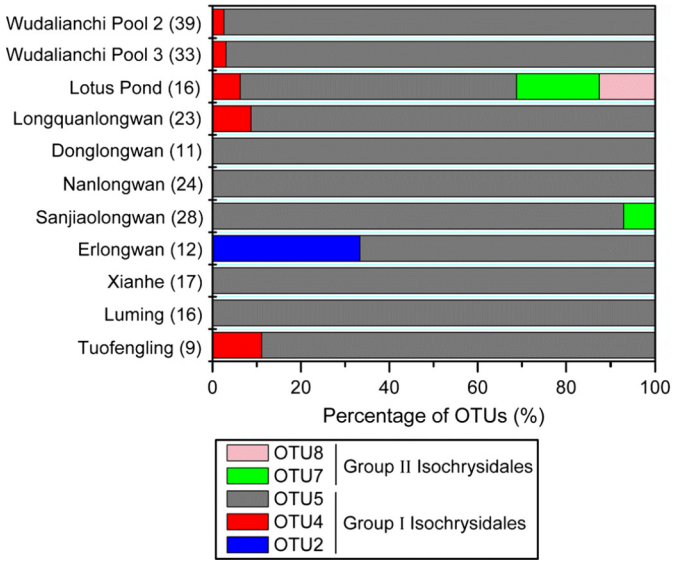

Fig. 2. Percentages of the five defined OTUs in the 11 haptophyte DNA-containing volcanic lakes of northeastern China. The OTUs 2, 4, and 5 are affiliated to "Greenland" subclade within Group I Isochrysidales, while OTUs 7 and 8 are affiliated to Group II Isochrysidales.

3. Results

3.1. The 18S rDNA-based haptophyte identification

All investigated 18 volcanic lake surface sediments yield sufficient total DNA concentrations, with a range from 7.7 to 25.7 μg per gram of raw sediments (Table S2). The haptophyte DNA bands from 11 of 18 lake sediments are amplified by PCR using haptophyte-specific primers (Coolen et al., 2004), indicating the occurrence of haptophytes in the 11 volcanic lakes (Fig. 1; Table S2). We identify five OTUs, which are defined as groups of DNA sequences with more than 98% similarity, from all obtained 228 haptophyte 18S rDNA sequences. The five OTUs are grouped with previously published OTUs 2, 4, 5, 7, and 8 from globally distributed lakes (Theroux et al., 2010) at 98% cut-off criterion, and are named accordingly for consistency (OTUs 2, 4, 5, 7, and 8). The 11 haptophyte DNA-containing lakes are dominated by OTU 5 (>~85%), although percentage of OTU 5 is slightly lower in Lotus pond and Erlongwan lakes (~60%; Fig. 2; Table S2). In particular, Donglongwan, Nanlongwan, Xianhe, and Luming host 100% OTU 5 based on the recovered DNA sequences.

The phylogenetic tree of haptophyte 18S rDNA sequences from the volcanic lakes is constructed using a representative sequence for each OTU along with available haptophyte gene sequences from the public GeoBank database (Fig. 3). The alkenone-producing haptophytes are phylogenetically classified into three distinct groups: Group I, Group II, and Group III, as first defined by Theroux et al. (2010). The OTUs 2, 4, and 5 are affiliated to the "Greenland" clade within Group I Isochrysidales, while OTUs 7 and 8 are clustered with Group II Isochrysidales. None of our statistically defined OTUs based on 228 haptophyte 18S rDNA sequences found in our samples are grouped at 98% cut-off criterion with previously published OTUs 1, 3, and 6 from globally distributed lakes (Theroux et al., 2010). We compare sequence data of our OTUs (OTUs 2, 4, 5, 7, and 8) with the published OTUs 1-8 from Theroux et al. (2010): OTUs 1-5 are affiliated to Group I and OTUs 6-8 are affiliated to Group II (Table S3). The OTU 2 in our volcanic lakes is closest to published OTU 2 from Greenland Lake BrayaSø with 99.3% similarity. The OTU 4 in our volcanic lakes shows 98% similarity with published OTU 4 from Lake BrayaSø. The OTU 5 in our volcanic

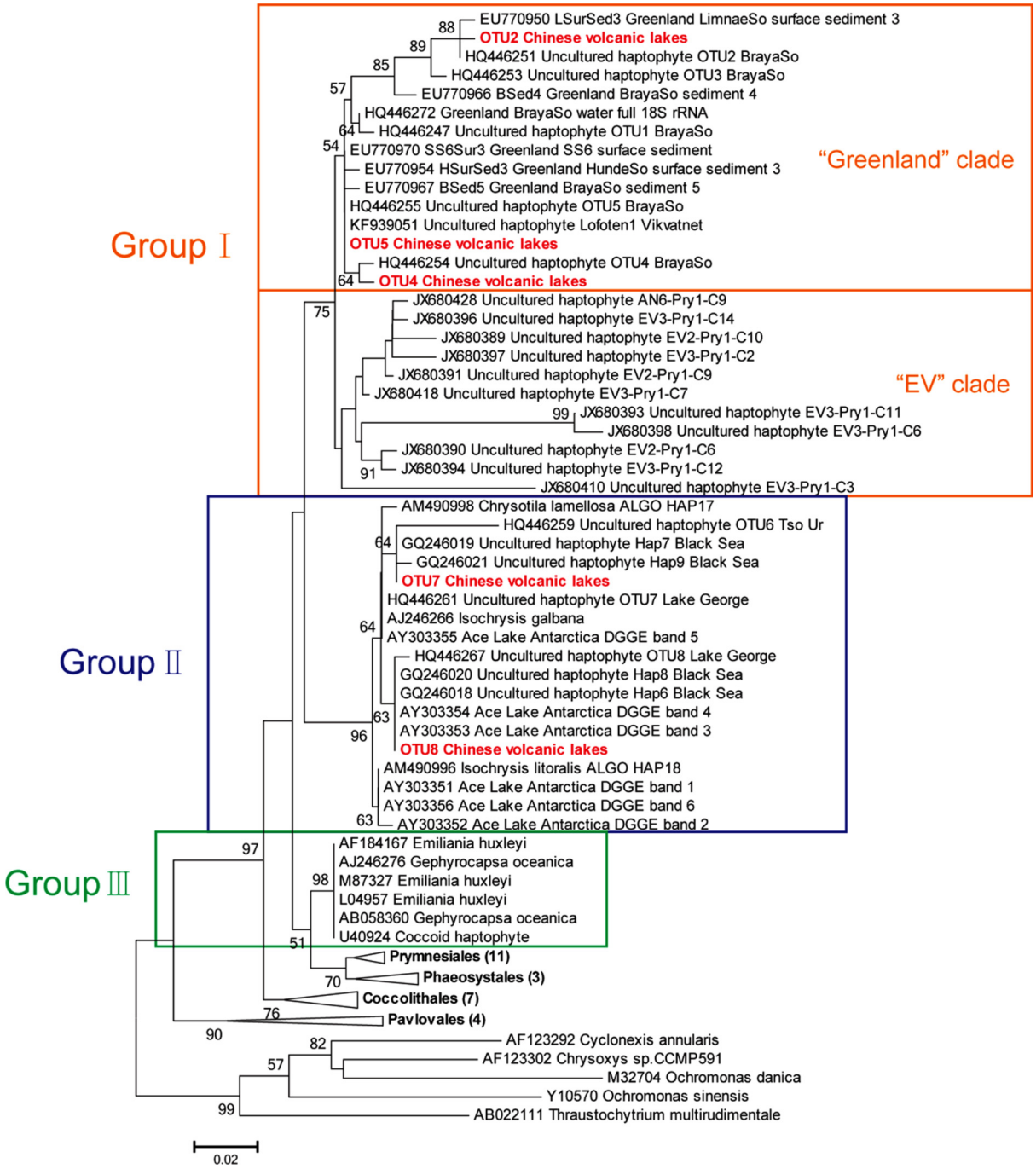

Fig. 3. Consensus neighbor-joining phylogenetic tree depicting 18S rRNA gene-inferred relatedness of haptophytes.

lakes matches 100% with published OTU 5 from Lake BrayaSø. The OTU 7 in our volcanic lakes is closely related to published OTU 7 from saline lakes with 99.3% similarity. The OTU 8 in our volcanic lakes is closely related to published OTU 8 from saline lakes with 99.6% similarity. Surprisingly, in the 11 haptophyte DNA-containing volcanic lakes, Lotus Pond and Sanjiaolongwan unexpectedly contain a mixture of Group I and Group II Isochrysidales, with small numbers of Group II sequences (Fig. 2; Table S2). Lotus Pond contains five Group II sequences (three OTU 7 sequences and two OTU 8 sequences) out of the total 16 recovered sequences and Sanjiaolongwan contains two Group II sequences (OTU 7 sequences) out of the total 28 recovered sequences, respectively. The other nine lakes contain only Group I Isochrysidales (OTUs 2, 4, and 5), all dominated by OTU 5 (~65%–100%; Fig. 2; Table S2).

3.2. LCA distributions

LCAs are detected in 11 of 18 volcanic lakes investigated in this study, fully corresponding to the occurrence of haptophyte DNA (Fig. 1; Table S1). The concentrations of C_{37}, C_{38}, and C_{39} LCAs range from 0.01 to 5.45 μg, 0.06 to 5.16 μg, and 0.00 to 0.63 μg per gram of dry sediments with average values of 1.23, 1.22, and 0.14 μg/g, respectively (Table S1). LCAs in Lotus Pond are very low in concentration and co-eluted with unknown compounds for identification and quantification of individual LCAs. LCA distributions in the other ten Group I-dominant volcanic lakes are characteristic of Group I-type LCA distributions, with relatively abundant $C_{37:4}$, the presence of $C_{37:3b}$ tri-unsaturated isomer and C_{38}Me LCAs, and RIK_{37} values of 0.5–0.6 (Figs. 4 and S1; Tables S1

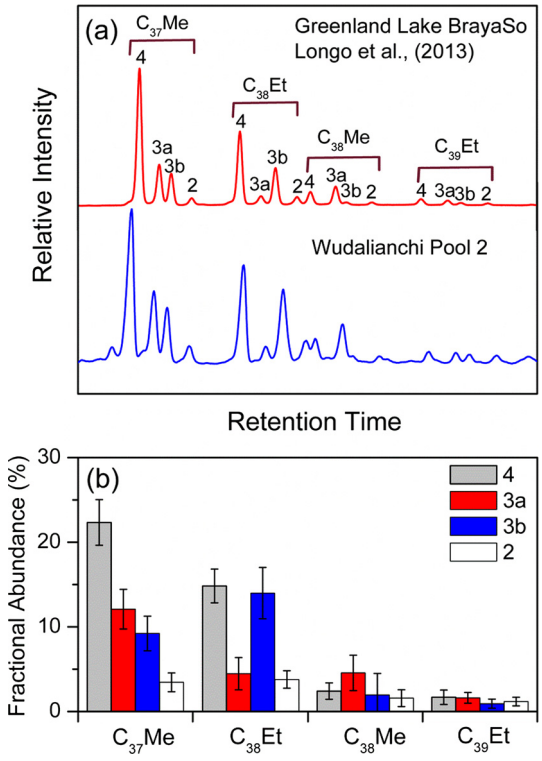

Fig. 4. (a) Partial gas chromatograms of LCAs from Greenland Lake BrayaSø (Longo et al., 2013) and Wudalianchi Pool 2. (b) Average fractional abundances of LCAs in investigated volcanic lakes with dominant Group I Isochrysidales (excluding Lotus Pond as its individual LCAs were not fully resolved on GC-FID).

and S5; Longo et al., 2016). DNA data further support the presence of Group I Isochrysidales in our volcanic lakes (Fig. 2; Table S2). The LCA distribution pattern in our lakes is highly consistent with those from Greenland Lake BrayaSø (Longo et al., 2013) that exclusively hosts Group I Isochrysidales (Fig. 4). Combined DNA and LCA data further confirm that RIK_{37} value is a reliable taxonomic indicator for Group I Isochrysidales.

3.3. Relationships between LCA concentrations and environmental factors

In order to identify the environmental controls on the occurrence and concentrations of LCAs, we performed two PCA analyses of total LCA concentrations and water chemistry data (Fig. 5). In the first PCA (including environmental parameters: pH, TN, and major ions), the first two principal components explain a total of 68.3% of the variance, with axis 1 explaining 42.4% of the variance (Fig. 5a). The analysis clearly shows that the concentrations of LCAs are inversely related to TN and major cations, especially Na^+, K^+, and Mg^{2+}. In the second PCA (including environmental parameters: trace elements), the first two principal components explain the 100% variance, with axis 1 explaining 91.4% of the variance (Fig. 5b). The concentrations of LCAs cannot be differentiated by the variance of the six trace elements (Fe, Mn, Zn, Cu, Mo, and Co). However, the absence of LCAs in Songshu and Buteha Tianchi coincides with high abundance of Fe, whereas the absence of LCAs in Yaoquanchi is correlated with high abundance of Zn, Mn and Mo (Fig. 5b).

4. Discussion

4.1. Widespread occurrence of Group I Isochrysidales in volcanic lakes of northeastern China

Our DNA results demonstrate that the 11 freshwater volcanic lakes (salinity: 0.02–0.18‰; Table S1) host Group I Isochrysidales with a dominant genotype that is closely related with the Greenland OTU 5 of the "Greenland" subclade (Fig. 2), as first defined by Theroux et al. (2010). The OTU 5 genotype of the "Greenland" subclade appears to occur extensively in freshwater lakes around the world, including Greenland, USA, Canada, and China (Theroux et al., 2010; Richter et al., 2019). Recently published Group I DNA sequences from freshwater Lake Vikvatnet in Norway (D'Andrea et al., 2016) and oligohaline Bothnian Bay in the Baltic Sea (Kaiser et al., 2019) are also most closely related to the Greenland OTU 5. Another subclade ("EV" subclade) within Group I Isochrysidales has also been identified in freshwater lakes in France using differently designed primers (Simon et al., 2013) and recently also found in many freshwater lakes around the world, including Alaska, Iceland, and Germany (Richter et al., 2019). However, we did not find the "EV" subclade in our volcanic lakes (Fig. 3), because this haptophyte clade cannot be amplified using the primers from Coolen et al. (2004) due to primer mismatch (Richter et al., 2019). Using high-throughput sequencing with a general eukaryotic primer, "EV" subclade has recently been found to co-exist with the "Greenland" subclade in virtually random percentages in freshwater lakes harboring Group I Isochrysidales, although in almost all cases the "Greenland" subclade dominates over the "EV" subclade (Richter et al., 2019). It is highly likely that the 11 volcanic lakes in the northeastern China contain "EV" subclade as well.

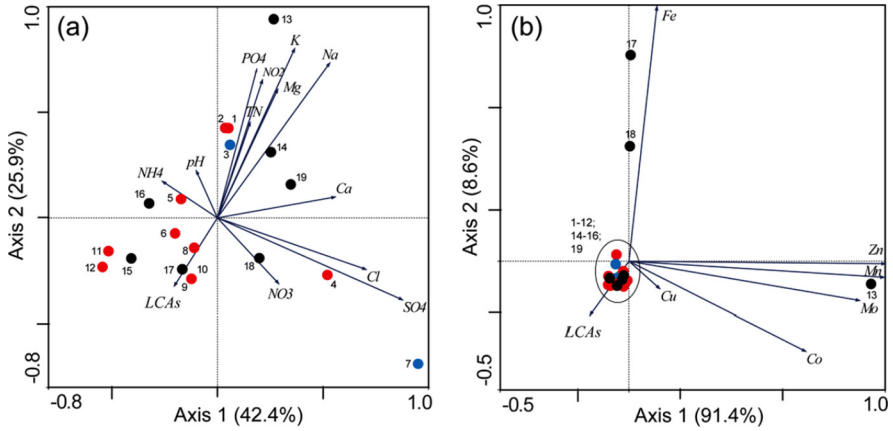

Fig. 5. PCA analysis showing the relationships between LCA concentrations and various water chemistry parameters. The red circles depict the lakes with only Group I Isochrysidales; the black circles illustrate the lakes that do not contain LCAs; the blue circles denote the lakes with mixture of Group I and II Isochrysidales. (1) Wudalianchi Pool 2; (2) Wudalianchi Pool 3; (3) Lotus Pond; (4) Longquanlongwan; (5) Donglongwan; (6) Nanlongwan; (7) Sanjiaolongwan; (8) Erlongwan; (9) Xianhe; (10) Xianhe; (11) Luming; (12) Tuofengling; (13) Yaoquanchi; (14) Dalongwan; (15) Xiaolongwan; (16) Wusulangzi; (17) Songshu; (18) Buteha Tianchi; (19) Tongxin Tianchi.

Surprisingly, we find that Lotus Pond (salinity: 0.07‰) and Sanjiaolongwan (salinity: 0.04‰) lakes also harbor small numbers of Group II Isochrysidales with five sequences out of total 16 recovered sequences and two sequences out of total 28 recovered sequences, respectively, although they still predominantly host Group I Isochrysidales (Fig. 2; Table S2). Previous survey of published DNA data suggests Group II Isochrysidales primarily occur in oligohaline to hyperhaline lakes with salinity >0.5‰, whereas freshwater lakes with salinity <0.5‰ appear to exclusively host Group I Isochrysidales (Longo et al., 2016). Our results extend, for the first time, the salinity range permissible for growth of Group II Isochrysidales to freshwater habitats with extremely low salinity (0.04 and 0.07‰). This indicates that, under certain specific environmental conditions, Group II Isochrysidales can also survive in freshwater lakes (steadily or transiently), and salinity is not the only parameter controlling the presence of Group II Isochrysidales.

In order to identify the environmental controls on the presence/absence of the five OTUs, we perform logistic regressions between the categorical presence/absence of OTUs and water chemistry data in 11 haptophyte DNA-containing volcanic lakes (Table S6). We define the water chemistry parameters as relatively important factors when the logistic regression is statistically significant ($p < 0.1$) (Table S6). The presence of Group II OTU 7 appears to be influenced by a combination of elevated concentrations of major ions NO_2^-, PO_4^{2-}, SO_4^{2-}, NH_4^+, and Mg^{2+}, as well as trace element Fe and Cu (Table S6). The presence of Group II OTU 8 appears to be influenced by a combination of elevated concentrations of major ions NO_2^-, NH_4^+, and Mg^{2+}, as well as trace element Fe (Table S6). Group II Isochrysidales appear to have more requirements for these major ions and trace elements relative to Group I Isochrysidales in these freshwater lakes. Importantly, we observe that both Lotus Pond and Sanjiaolongwan lakes containing small numbers of Group II Isochrysidales sequences (OTU 7 and 8) are fully developed tourist sites with direct discharge of untreated sewage into the lakes (Fig. S2). This may largely result in the relatively high concentrations of these major ions and trace elements in local water masses surrounding the discharging outlets, which could trigger a spontaneous growth of Group II Isochrysidales. Our results also suggest that Group II Isochrysidales may stay dormant in certain form in these lakes and could start to grow when environmental conditions are favorable.

Among the two volcanic lakes containing small numbers of Group II sequences, LCAs of Lotus pond are very low in concentration and poorly resolved chromatographically (Tables S1 and S5), whereas Sanjiaolongwan shows the characteristic Group I LCA distributions with RIK_{37} values of 0.6 (Tables S1 and S5): this value falls within the previously proposed Group I RIK_{37} range (Longo et al., 2016). This indicates that the contribution of Group II Isochrysidales to the total LCA inventory is relatively small in Sanjiaolongwan and has very limited impact on the sedimentary LCA distributions. Group II Isochrysidales may have grown transiently in response to inputs of sewage surrounding the outlet discharge points. The RIK_{37} values in the other nine LCA-containing volcanic lakes range from 0.5 to 0.6 (Table S1; Fig. S1), which is consistent with the presence of Group I Isochrysidales (Longo et al., 2016, 2018). The overall consistency between LCA distributions and DNA results further supports that the RIK_{37} index is a reliable taxonomic indicator for Group I Isochrysidales.

4.2. New constrains on the ideal pH values for Group I Isochrysidales

In northern Alaskan freshwater lakes, the concentrations of Group I LCAs are positively related with pH in the range of 6.2 to 8.5 (Longo et al., 2016). Our samples of volcanic lakes in northeastern China extend to an even higher pH range from 7.17 to 9.99 (Table S1). The very high pH values of some lakes in the volcanic fields of northeastern China may result from efficient weathering of the alkali basalt bedrock, especially olivine (Chen et al., 2007), that can release large amounts of OH^- anions:

$$(Mg, Fe)_2SiO_4 + 2H_2O + 2CO_2 = MgCO_3 + FeCO_3 + H_4SiO_4$$

$$MgCO_3 + H_2O = Mg^{2+} + HCO_3^- + OH^-$$

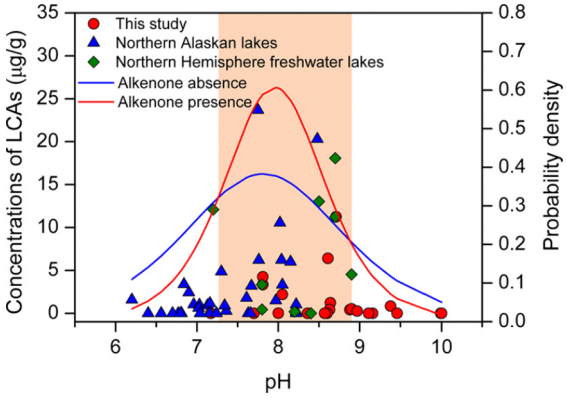

Fig. 6. Concentrations of Group I LCAs vs. pH, and logistic probability density for the presence and absence of Group I LCAs. The data of northern Alaskan lakes is from Longo et al. (2016) and the data of Northern Hemisphere freshwater lakes (surface sediments) is from Longo et al. (2018). Red bars represent our proposed ideal pH range of 7.3–8.8 for Group I Isochrysidales.

Here we combine our data with those from northern Alaska lakes (Longo et al., 2016), Northern Hemisphere freshwater lakes (nine surface sediments; Longo et al., 2018), and three additional volcanic lakes (Huguangyan, Southern China; Santiago, Azores; Congro, Azores) to further constrain the effect of pH values on the occurrence and abundance of Group I LCAs (Fig. 6; Table S7). We find that the high concentrations of Group I LCAs tend to occur in moderately alkaline lakes with pH ~7.3–8.8, and the logistic probability density functions display the higher likelihood of the presence (0.25–0.61) of Group I LCAs than the absence (0.25–0.38) of Group I LCAs within this pH range (Fig. 6; Table S7). Lake BrayaSø in southwestern Greenland is renowned for containing the highest LCA concentration (11.9 mg/g; D'Andrea and Huang, 2005) in the surface sediment among all lake and ocean sediment samples ever studied: its water pH is 8.4, which is within the range we propose here (D'Andrea and Huang, 2005). Nine (Longquanlongwan, Donglongwan, Nanlongwan, Luming, Xiaolongwan, Wusulangzi, Tongxin Tianchi, Santiago, and Congro) of our samples have exceptionally high pH values (>8.8): these lakes contain very low LCA concentrations or no LCAs (Table S1; Fig. 6). Our results indicate that extraordinarily high pH (>~8.8) adversely affects the growth of Group I Isochrysidales.

4.3. Impact of nutrients, major ions, and trace elements on Group I Isochrysidales

In addition, our PCA analyses indicate that the decreased nutrient TN and concentrations of the major ions, especially K^+, Na^+, and Mg^{2+}, are important for promoting the occurrence and abundance of Group I LCAs in our volcanic lakes (Fig. 5a). The two three-dimensional diagrams clearly show the concentrations of Group I LCAs generally increase with decreased concentrations of TN and major ions (K^+, Na^+, and Mg^{2+}) (Fig. S3), suggesting that the Group I Isochrysidales may preferentially thrive in oligotrophic freshwater conditions with reduced concentrations of major ions (especially K^+, Na^+, and Mg^{2+}). This is in agreement with previous results from northern Alaskan freshwater lakes showing that the Group I LCAs are generally absent from eutrophic lakes with relatively high C/N ratios and concentrations of dissolved organic

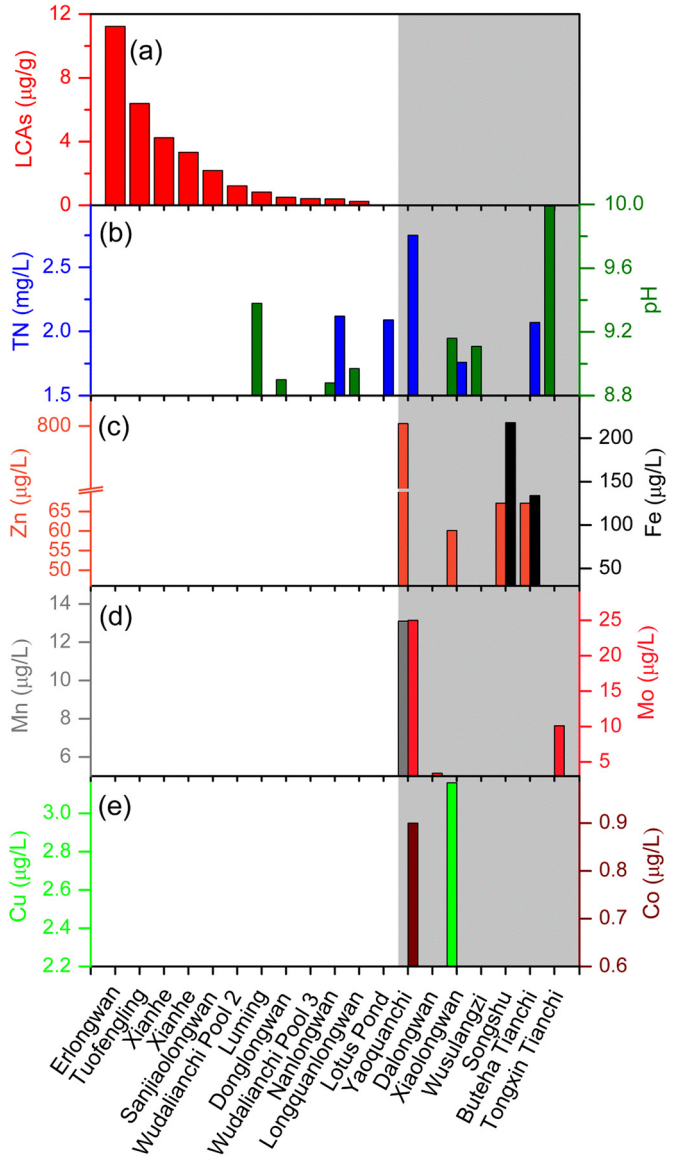

Fig. 7. Comparisons among concentrations of LCAs, TN, and trace elements (Zn, Fe, Mn, Mo, Cu and Co), as well as pH in our volcanic lakes.

carbon and chlorophyll (Longo et al., 2016). We cannot, however, exclude the possibility that the observed low concentrations of nutrients in lakes harboring Group I Isochrysidales is due to, at least in part, the efficient use of nutrients by the primary producers.

Nevertheless, not all lakes with the proper pH (i.e., between 7.3 and 8.8) and relatively low concentrations of TN and major ions (K^+, Na^+, and Mg^{2+}) contain LCAs (Figs. 6 and S3), suggesting that additional environmental factors play critical roles in determining the absence of Group I LCAs. We further compare the LCA concentrations with pH, TN, and trace elements (Zn, Fe, Mn, Mo, Cu, and Co) (Fig. 7). We find that the seven lakes (Yaoquanchi, Dalongwan, Xiaolongwan, Wusulangzi, Songshu, Buteha Tianchi, and Tongxin Tianchi) containing no LCAs have significantly elevated concentrations of one or more of six trace elements, except for Wusulangzi (Fig. 7). For example, Yaoquanchi has the highest concentrations of Zn (804 μg/L), Mn (13.1 μg/L), Mo (25.0 μg/L), and Co (0.9 μg/L) among all study lakes. Xiaolongwan has the highest concentration of Cu (3.2 μg/L); and Songshu has the highest concentration of Fe (218 μg/L) among all study lakes (Fig. 7; Table S4). Our results thus suggest that excessive concentrations of trace elements may be critical factors resulting in the absence of Group I LCAs, although the specific factors responsible for the absence of LCAs in Wusulangzi are currently unclear (e.g., could be due to the elevated concentration of another trace element we did not measure). More studies of freshwater lakes are required to further confirm the influence of trace elements on the absence of Group I LCAs in the future. However, our existing data do not allow us to fully exclude other lake environmental conditions (e.g., competition between different algal species) as factors responsible for the absence of LCAs in freshwater lakes with appropriate pH.

Trace elements, such as Fe, Zn, Mn, and Cu, play an essential role in a variety of metabolic and structural functions for microalgae, as they makeup many enzymes and proteins (e.g. Anderson, 2005). However, excessive amount of certain trace elements may inhibit the growth of microalgae. For example, Zn can inhibit the enzymatic activity of protochlorophyllide reductase, which is involved in the reductive steps of the biosynthetic pathway of photosynthetic pigments (e.g. De Filippis et al., 1981). Cu can affect photosynthetic electron transfer systems by inhibiting ferredoxin-catalyzed reactions (Samson et al., 1988), and can reduce cell defense mechanisms against H_2O_2 and oxygen-free radicals by inhibiting the enzyme catalase (Stauber and Florence, 1987). Mn toxicity can trigger oxidative stress by generating harmful reactive oxygen species, and cause some metabolic alterations and macromolecular damage that disrupt cell homeostasis (Millaleo et al., 2010). Excessive concentrations of certain trace elements may thus be toxic to Group I Isochrysidales.

Unfortunately, no studies have successfully isolated and cultured the Group I Isochrysidales. Part of the reason for the difficulty in laboratory culturing of Group I Isochrysidales may be that concentrations of nutrients, major ions, and trace elements in culture are too high. Microalgae growth in culture usually depends on an adequate supply of essential macronutrient elements (C, N, P, and Si) and major ions (K^+, Ca^{2+}, Mg^{2+}, Na^+, SO_4^{2-}, and Cl^-) as well as a certain amount of micronutrient metals (Fe, Mn, Zn, Cu, Mo, and Co) (Anderson, 2005). However, for the Group I Isochrysidales, our results suggest that excessive additions of TN, major ions (especially K^+, Na^+, and Mg^{2+}), and trace elements may adversely affect the growth of these microalgae. Therefore, culture experiments for Group I Isochrysidales may benefit from using natural (or artificial) waters containing appropriate levels of major ions and trace elements. It is also possible, when isolated, that Group I Isochrysidales would thrive in high nutrient conditions. One possible reason for their prevalence in oligotrophic natural waters is that they outcompete other organisms under such conditions.

4.4. R3b as a potential winter temperature proxy

The Group I U^K_{37} proxy has been demonstrated to be well correlated with in situ water temperature from SPM samples of water column in Lake BrayaSø (D'Andrea et al., 2011) and Toolik Lake (Longo et al., 2016) as well as sediment trap samples in Lake Vikvatnet (D'Andrea et al., 2016). However, there are slight differences in y-intercept and/or slope for the three U^K_{37}-temperature calibrations from different regions (Fig. S4). Sediment trap data indicate that the maximum production of Group I LCAs occurs during ice melt and isothermal mixing in various freshwater lakes across different geographic location, including Lake BrayaSø in southwestern Greenland (D'Andrea et al., 2011), Lake Vikvatnet in Norway (D'Andrea et al., 2016), and Toolik Lake and Lake E5 in northern Alaska (Longo et al., 2018). The sedimentary Group I LCAs would mainly record the lake water temperature during the winter-spring transitional season, which is affected by lake ice thickness in the winter and the rate of lake ice melt and warming in the spring (Longo et al., 2018). In addition, the bloom timing of Group I Isochrysidales during the winter-spring transitional season may also be affected by light intensity associated mainly with absorbed

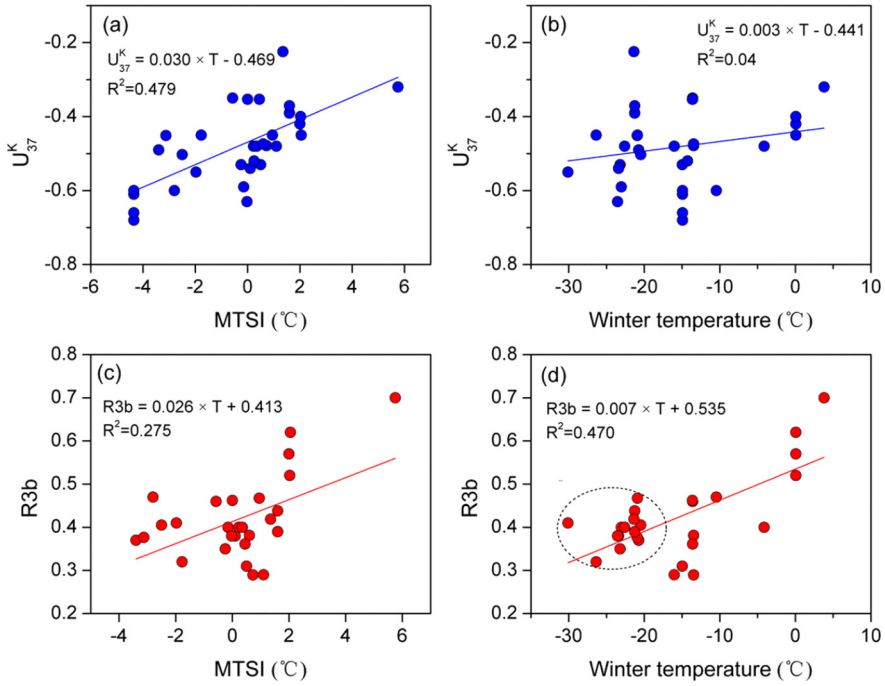

Fig. 8. Group I U^K_{37} and R3b (Equation (2)) values from surface sediments in our volcanic lakes and published Northern Hemisphere freshwater lakes (Longo et al., 2018) vs. mean temperature of the spring isothermal season (MTSI) and winter temperature.

solar radiation and ice thickness over a large region (e.g. Bleiker and Schanz, 1997).

The R3b index (Equation (2)) has also been proposed to have potential as a new temperature proxy as it is also well correlated with in situ water temperature (Longo et al., 2018). When combined with published Group I LCA data in temperature calibrations from Northern Hemisphere freshwater lake surface sediments (Table S8; Longo et al., 2018), Group I U^K_{37} values are most significantly correlated with MTSI (Figs. 8a and 8b). In this study, we find that R3b values, however, show better correlations with December ($R^2 = 0.464$), January ($R^2 = 0.502$), and February ($R^2 = 0.427$) temperatures than with other months (Table S9; Fig. S5), and are more sensitive to the mean winter temperature ($R^2 = 0.470$), rather than MTSI ($R^2 = 0.275$). However, we note that R3b becomes relatively insensitive to the winter temperatures when temperatures fall below ~−20 °C (Figs. 8c and 8d).

In addition to air temperature, maximum ice thickness is an important determinant of lake water temperature during the winter-spring transitional season (e.g. Fang and Stefan, 1996). We calculate the maximum ice thickness (MIT) of our volcanic lakes and the Northern Hemisphere freshwater lakes (Longo et al., 2018) using the following formula (Williams and Stefan, 2006; Table S8):

$$\text{MIT (cm)} = -7.904 \times T + -0.913 \times \text{LAT} + 0.014 \times \text{EL} + 0.0009 \times \text{SA} + 0.229 \times \text{MD} + 100.5 \quad (3)$$

where T = mean air temperature (°C) from September 1 to June 30; LAT = latitude (in °N); EL = elevation (m); SA = surface area (km^2); and MD = mean depth (m). The MIT is mainly determined by winter temperature although latitude, elevation, surface area and mean depth of lakes have small influence on the MIT (Fig. 9a). Generally, R3b values are negatively correlated with maximum ice thickness ($R^2 = 0.626$) when the ice is thinner than ~100 cm: notably correlation disappears when the modeled maximum ice thickness exceeds ~100 cm (Fig. 9b). This may be largely related to the duration of ice melt as thicker ice would result in longer ice-out season, resulting in lake water experiencing longer duration of relatively cold water temperature when Group I Isochrysidales are starting to bloom. However, when ice is too thick (>~100 cm), the correlation weakens and R3b values are unresponsive, suggesting that the growth of Group I Isochrysidales may be impeded by diminished light intensity through the ice.

Alternatively, light intensity under ice during winter-spring transitional season may affect the bloom timing of Group I Isochrysidales. Absorbed solar radiation and ice thickness are two major factors determining the light intensity over a large region (e.g. Katlein et al., 2015). We calculated the ice surface albedo of our volcanic lakes and the Northern Hemisphere freshwater lakes (Longo et al., 2018) using the following model of ice surface albedo (Svacina et al., 2014):

$$a_i = c_1 \times h_i^{0.28} + 0.08 \quad (T_s < T_f) \quad (4)$$

where a_i is the ice surface albedo, c_1 is a constant equal to 0.44 $m^{-0.28}$, h_i is the ice thickness (m), T_s is the ice surface temperature, and T_f is the freezing temperature (273.15 K). The winter-spring absorbed solar radiation (ASR) is calculated by: ASR = solar radiation × $(1 - a_i)$ (Table S8). We find that R3b values generally decrease with increasing maximum ice thickness and decreasing winter-spring ASR when mean winter temperatures are >~−20 °C (Fig. 9c), indicating that changes in R3b may be associated with light intensity. We speculate that higher light intensity under ice during winter-spring transitional season may trigger the earlier growth of Group I Isochrysidales in the early winter-spring transitional season or even in the winter, which may lead to more sensitive response of R3b to winter temperature in the relatively warm regions (mean winter temperature >~−20 °C).

5. Conclusions

We find that 11 of 18 freshwater volcanic lakes of northeastern China host Group I Isochrysidales with a dominant genotype that is closely related to the Greenland OTU 5 of “Greenland” subclade. Surprisingly, two freshwater lakes (Lotus Pond and Sanjiaolongwan) harbor a small number of Group II Isochrysidales sequences, which were likely promoted by pollution from human activities

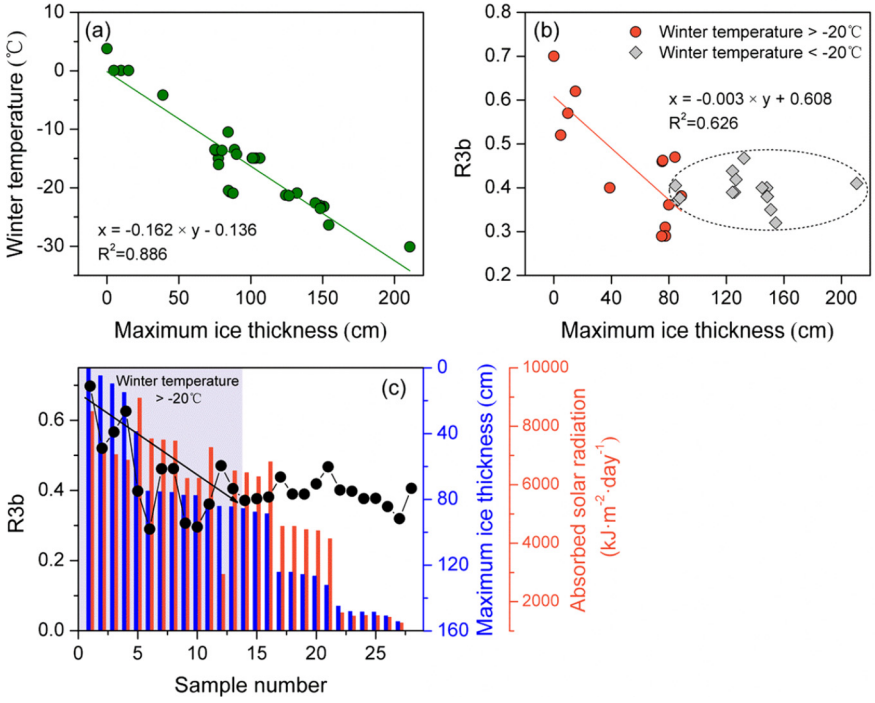

Fig. 9. Winter temperature (a) and R3b values (b) vs. lake maximum ice thickness in our volcanic lakes and published Northern Hemisphere freshwater lakes (Longo et al., 2018). (c) R3b vs. lake maximum ice thickness and winter-spring absorbed solar radiation in our volcanic lakes and published Northern Hemisphere freshwater lakes (Longo et al., 2018).

with enhanced nutrient concentrations. All LCA profiles in surface sediments are characterized by Group I-type LCA distributions even when small numbers of Group II DNA sequences can be detected.

Our new LCA data define an upper limit (∼8.8) of pH range that favors the growth of Group I Isochrysidales. Combined with analyses of detailed water chemistry parameters, our results indicate that Group I Isochrysidales may preferentially thrive in the optimal pH range (∼7.3–8.8) and oligotrophic freshwater environments with reduced concentrations of major cations (especially K^+, Na^+, and Mg^{2+}). Importantly, we find that excessive concentrations of certain trace elements (e.g. Zn, Fe, Mn, Mo, Cu, and Co) may inhibit the growth of Group I Isochrysidales probably due to their toxic effect, despite these lakes having the optimal pH and oligotrophic conditions.

We propose, for the first time, that Group I R3b has potential as a winter temperature proxy in regions with mean winter temperature $>\sim -20\,^{\circ}C$. We also find a strong correlation between R3b and calculated maximum ice thickness when the ice is thinner than ∼100 cm. We do acknowledge that winter temperature is likely the primary control on the maximum ice thickness, however. The potential applications of Group I R3b as winter temperature proxy could fill the important gap in paleoclimatology that majority of existing proxies (including organic biomarker proxies) reflect conditions in the summer growth season.

Acknowledgements

This work was supported by the National Natural Science Foundation of China (No. 41573113 award to Y. Huang, No. 41702187 award to Y. Yao, No. 41602193 award to J. Zhao) and the project from the State Key Laboratory of Loess and Quaternary Geology in the Institute of Earth Environment, Chinese Academy of Sciences (SKLLQGPY1704), and the U.S. National Science Foundation (No. EAR-1122749, PLR-1503846, EAR-1502455, EAR-1762431 award to Y. Huang). We thank J. Jing and Longwan National Nature Reserve Administration of Jilin Province for assistance during sample collection, L. Wang and P. Raposeiro for providing the Huguangyan and Azorean volcanic lake samples, C. Zhang for help on drawing of contour map, and H. Xie, J. Liang, and S. Liao for discussions. We are also grateful for the constructive comments and suggestions of two anonymous reviewers that are very helpful for improving our manuscript as well as for future studies.

Appendix A. Supplementary material

Supplementary material related to this article can be found online at https://doi.org/10.1016/j.epsl.2019.115792.

References

Anderson, R.A., 2005. Algal Culturing Techniques. Elsevier Science and Technology Books, Academic Press.

Bleiker, W., Schanz, F., 1997. Light climate as the key factor controlling the spring dynamics of phytoplankton in Lake Zürich. Aquat. Sci. 59, 135–157.

Brassell, S.C., Eglinton, G., Marlowe, I.T., Pflaumann, U., Sarnthein, M., 1986. Molecular stratigraphy: a new tool for climatic assessment. Nature 320, 129–133.

Chen, Y., Zhang, Y., Graham, D., Su, S., Deng, J., 2007. Geochemistry of Cenozoic basalts and mantle xenoliths in Northeast China. Lithos 1–2, 108–126.

Chu, G., Sun, Q., Li, S., Zheng, M., Jia, X., Lu, C., Liu, J., Liu, T., 2005. Long-chain alkenone distributions and temperature dependence in lacustrine surface sediments from China. Geochim. Cosmochim. Acta 69, 4985–5003.

Conte, M.H., Eglinton, G., Madureira, L.A.S., 1992. Long chain alkenones and alkyl alkenoates as paleotemperature indicators: their production, flux and early sedimentary diagenesis in the Eastern North Atlantic. Org. Geochem. 19, 287–298.

Conte, M.H., Thompson, A., Lesley, D., Harris, R.P., 1998. Genetic and physiological influences on the alkenone/alkenoate versus growth temperature relationship in *Emiliania huxleyi* and *Gephyrocapsa oceanica*. Geochim. Cosmochim. Acta 62, 51–68.

Conte, M.H., Sicre, M., Ruhlemann, C., Weber, J.C., Schulte, S., Schulz-Bull, D., Blanz, T., 2006. Global temperature calibration of the alkenone unsaturation index ($U^{K'}_{37}$) in surface waters and comparison with surface sediments. Geochem. Geophys. Geosyst. 7. https://doi.org/10.1029/2005GC001054.

Coolen, M.J.L., Muyzer, G., Rijpstra, W.I.C., Schouten, S., Volkman, J.K., Sinninghe Damsté, J.S., 2004. Combined DNA and lipid analyses of sediments reveal changes in Holocene haptophyte and diatom populations in an Antarctic lake. Earth Planet. Sci. Lett. 223, 225–239.

D'Andrea, W.J., Huang, Y., 2005. Long chain alkenones in Greenland lake sediments: Low $\delta^{13}C$ values and exceptional abundance. Org. Geochem. 36, 1234–1241.

D'Andrea, W.J., Lage, M., Martiny, J.B.H., Laatsch, A.D., Amaral-Zettler, L.A., Sogin, M.L., Huang, Y., 2006. Alkenone producers inferred from well-preserved 18S rDNA in Greenland lake sediment. J. Geophys. Res. 111. https://doi.org/10.1029/2005JG000121.

D'Andrea, W.J., Huang, Y., Fritz, S.C., Anderson, N.J., 2011. Abrupt Holocene climate change as an important factor for human migration in West Greenland. Proc. Natl. Acad. Sci. USA 108, 9765–9769.

D'Andrea, W.J., Theroux, S., Bradley, E.S., Huang, X., 2016. Does phylogeny control U^{K}_{37}-temperature sensitivity? Implications for lacustrine alkenone paleothermometry. Geochim. Cosmochim. Acta 175, 168–180.

De Filippis, L.F., Hampp, R., Ziegler, H., 1981. The effects of sublethal concentrations of zinc, cadmium and mercury on Euglena. Arch. Microbiol. 101, 407–411.

de Leeuw, J.W., van der Meer, F.W., Rijpstra, W.I.C., Schenck, P.A., 1980. On the occurrence and structural identification of long chain unsaturated ketones and hydrocarbons in sediments. Phys. Chem. Earth 12, 211–217.

Eglinton, G., Bradshaw, S.A., Rosell, A., Sarnthein, M., Pflaumann, U., Tiedemann, R., 1992. Molecular record of secular sea surface temperature changes on 100-year timescales for glacial terminations I, II, IV. Nature 356, 423–426.

Fang, X., Stefan, H.G., 1996. Long-term lake water temperature and ice cover simulations/measurements. Cold Reg. Sci. Technol. 24, 289–304.

Fick, S.E., Hijmans, R.J., 2017. WorldClim 2: new 1-km spatial resolution climate surfaces for global land areas. Int. J. Climatol. 37, 4302–4315.

Filippova, A., Kienast, M., Frank, M., Schneider, R.R., 2016. Alkenone paleothermometry in the North Atlantic: a review and synthesis of surface sediment data and calibrations. Geochem. Geophys. Geosyst. https://doi.org/10.1002/2015GC006106.

Freeman, K.H., Wakeham, S.G., 1992. Variations in the distributions and isotopic composition of alkenones in Black Sea particles and sediments. Org. Geochem. 19, 277–285.

Kaiser, J., Wang, K.J., Rott, D., Li, G., Zheng, Y., Amaral-Zettler, L., Arz, H.W., Huang, Y., 2019. Changes in long chain alkenone distribution and Isochrysidales groups along the Baltic Sea salinity gradient. Org. Geochem. 127, 92–103.

Karger, D.N., Conrad, O., Böhner, J., Kawohl, T., Kreft, H., Soria-Auza, R.W., Zimmermann, N.E., Linder, H.P., Kessler, M., 2017. Climatologies at high resolution for the Earth's land surface areas. Sci. Data 4, 170122.

Katlein, C., Arndt, S., Nicolaus, M., Perovich, D.K., Jakuba, M.V., Suman, S., Elliott, S., Whitcomb, L.L., McFarland, C.J., Gerdes, R., Boetius, A., German, C.R., 2015. Influence of ice thickness and surface properties on light transmission through Arctic sea ice. J. Geophys. Res., Oceans 120, 5932–5944.

Liu, W., Liu, Z., Wang, H., He, Y., Wang, Z., Xu, L., 2011. Salinity control on long-chain alkenone distributions in lake surface waters and sediments of the northern Qinghai-Tibetan Plateau, China. Geochim. Cosmochim. Acta 75, 1693–1703.

Longo, W.M., Dillon, J.T., Tarozo, R., Salacup, J.M., Huang, Y., 2013. Unprecedented separation of long chain alkenones from gas chromatography with a poly(trifluoropropylmethylsiloxane) stationary. Org. Geochem. 65, 94–102.

Longo, W.M., Theroux, S., Gibin, A.E., Zheng, Y., Dillon, J.T., Huang, Y., 2016. Temperature calibration and phylogenetically distinct distributions for freshwater alkenones: evidence from northern Alaskan lakes. Geochim. Cosmochim. Acta 180, 177–196.

Longo, W.M., Huang, Y., Yao, Y., Zhao, J., Giblin, A.E., Wang, X., Zech, R., Haberzettl, T., Jardillier, L., Toney, J., Liu, Z.H., Krivonogov, S., Kolpakova, M., Chu, G.Q., D'Andrea, W.J., Harada, N., Nagashima, K., Sato, M., Yonenobu, H., Yamada, K., Gotanda, K., Shinozuka, Y., 2018. Widespread occurrence of distinct alkenones from Group I haptophytes in freshwater lakes: implications for paleotemperature and paleoenvironmental reconstructions. Earth Planet. Sci. Lett. 492, 239–250.

Marlowe, I.T., Green, J.C., Neal, A.C., Brassell, S.C., Eglinton, G., Course, P.A., 1984. Long chain (n-C_{37}–C_{39}) alkenones in the Prymnesiophyceae: distribution of alkenones and other lipids and their taxonomic significance. Brit. Phycol. J. 19, 203–216.

Millaleo, R., Reyes-Díaz, M., Ivanov, A.G., Mora, M.L., Alberdi, M., 2010. Manganese as essential and toxic element for plants: transport, accumulation and resistance mechanisms. J. Plant Nutr. Soil Sci. 10, 476–494.

Nakamura, H., Sawada, K., Araie, H., Suzuki, I., Shiraiwa, Y., 2014. Long chain alkenes, alkenones and alkenoates produced by the haptophyte alga *Chrysotila lamellose* CCMP1307 isolated from a salt marsh. Org. Geochem. 66, 90–97.

Plancq, J., McColl, J.L., Bendle, J.A., Seki, O., Couto, J.M., Henderson, A.C.G., Yamashita, Y., Kawamura, K., Toney, J.L., 2018. Genomic identification of the long-chain alkenone producer in freshwater Lake Toyoni, Japan: implication for temperature reconstructions. Org. Geochem. 125, 189–195.

Prahl, F.G., Wakeham, S.G., 1987. Calibration of unsaturation patterns in long-chain ketone compositions for palaeotemperature assessment. Nature 330, 367–369.

Richter, N., Longo, W.M., George, S., Shipunova, A., Huang, Y., Amaral-Zettler, L., 2019. Phylogenetic diversity in freshwater-dwelling Isochrysidales haptophytes with implications for alkenone production. Geobiology. https://doi.org/10.1111/gbi.12330.

Samson, G., Morisette, J.C., Popovic, R., 1988. Copper quenching of the variable fluorescence in *Dunaliella tertiolecta*: new evidence for a copper inhibition effect on PSII photochemistry. Photochem. Photobiol. 48, 329–332.

Schloss, P.D., Handelsman, J., 2005. Introducing DOTUR, a computer program for defining operational taxonomic units and estimating species richness. Appl. Environ. Microbiol. 71, 1501–1506.

Simon, M., López-García, P., Moreira, D., Jardillier, L., 2013. New haptophyte lineages and multiple independent colonizations of freshwater ecosystems. Environ. Microbiol. Rep. 5, 322–332.

Stauber, J.L., Florence, T.M., 1987. Mechanism of toxicity of ionic copper and copper complexes to algae. Mar. Biol. 94, 511–519.

Svacina, N.A., Duguay, C.R., King, J.M.L., 2014. Modelled and satellite-derived surface albedo of lake ice–part II: evaluation of MODIS albedo products. Hydrol. Process. 28, 4562–4572.

Theroux, S., D'Andrea, W.J., Toney, J., Amaral-Zettler, L., Huang, Y., 2010. Phylogenetic diversity and evolutionary relatedness of alkenone-producing haptophyte algae in lakes: implications for continental paleotemperature reconstructions. Earth Planet. Sci. Lett. 300, 311–320.

Toney, J.L., Huang, Y., Fritz, S.C., Baker, P.A., Grimm, E., Nyren, P., 2010. Climatic and environmental controls on the occurrence and distributions of long chain alkenones in lakes of the interior United States. Geochim. Cosmochim. Acta 74, 1563–1578.

Volkman, J.K., Eglinton, G., Corner, E.D.S., Forsberg, T.E.V., 1980. Long-chain alkenes and alkenones in the marine coccolithophorid *Emiliania huxleyi*. Phytochemistry 19, 2619–2622.

Wang, L., Long, W.M., Dillon, J.T., Zhao, J., Zheng, Y., Moros, M., Huang, Y., 2019. An efficient approach to eliminate steryl ethers and miscellaneous esters/ketones for gas chromatographic analysis for alkenones and alkenoates. J. Chromatogr. 1596, 175–182.

Williams, S.G., Stefan, H.G., 2006. Modeling of lake ice characteristics in North America using climate, geography, and lake bathymetry. J. Cold Reg. Eng. 20, 140–167.

Yao, Y., Zhao, J., Bauersachs, T., Huang, Y., 2019. Effect of water depth on the TEX_{86} proxy in volcanic lakes of northeastern China. Org. Geochem. 129, 88–98.

Zhao, J., An, C., Longo, W.M., Dillon, J.T., Zhao, J., Shi, C., Chen, Y., Huang, Y., 2014. Occurrence of extended chain length C_{41} and C_{42} alkenones in hypersaline lakes. Org. Geochem. 75, 48–53.

Zhao, J., Thomas, E.K., Yao, Y., DeAraujo, J., Huang, Y., 2018. Major increase in winter and spring precipitation during the Little Ice Age in the westerly dominated northern Qinghai-Tibetan Plateau. Quat. Sci. Rev. 199, 30–40.

Zheng, Y., Huang, Y., Andersen, R.A., Amaral-Zettler, L.A., 2016. Excluding the diunsaturated alkenone in the U^{K}_{37} index strengthens temperature correlation for the common lacustrine and brackish-water haptophytes. Geochim. Cosmochim. Acta 175, 36–46.

Zheng, Y., Tarozo, R., Huang, Y., 2017. Optimizing chromatographic resolution for simultaneous quantification of long chain alkenones, alkenoates and their double bond positional isomers. Org. Geochem. 111, 136–143.

Zheng, Y., Heng, P., Conte, M.H., Vachula, R.S., Huang, Y., 2019. Systematic chemotaxonomic profiling and novel paleotemperature indices based on alkenones and alkenoates: potential for disentangling mixed species input. Org. Geochem. 128, 26–41.

Zink, K., Leythaeuser, D., Melkonian, M., Schwark, L., 2001. Temperature dependency of long-chain alkenone distributions in Recent to fossil limnic sediments and in lake waters. Geochim. Cosmochim. Acta 65, 253–265.